

**Primary and secondary red bed magnetization
constrained by fluvial intraclasts**

Nicholas L. Swanson-Hysell¹, Luke M. Fairchild¹, Sarah P. Slotznick¹

¹Department of Earth and Planetary Science, University of California, Berkeley, CA, USA

Key Points:

- Red siltstone intraclasts reveal two ancient magnetizations held by hematite – one acquired before redeposition and the other after burial
- Fine-grained hematite spans from superparamagnetic to single domain leading to a wide range of unblocking temperatures and coercivities
- Detrital hematite thermally unblocks in a narrow high temperature range that can be isolated through high-resolution thermal demagnetization

12 **Abstract**

13 The magnetization of hematite-bearing sedimentary rocks provides critical records
 14 of geomagnetic reversals and paleogeography. However, the timing of hematite remanent
 15 magnetization acquisition is typically difficult to constrain. While detrital hematite in
 16 sediment can lead to a primary depositional remanent magnetization, alteration of min-
 17 erals through interaction with oxygen can lead to the post-depositional formation of hematite.
 18 In this study, we use exceptionally-preserved fluvial sediments within the 1.1 billion-year-
 19 old Freda Formation to gain insight into the timing of hematite remanence acquisition
 20 and its magnetic properties. This deposit contains siltstone intraclasts that were eroded
 21 from a coexisting lithofacies and redeposited within channel sandstone. Thermal demag-
 22 netization, petrography and rock magnetic experiments on these clasts reveal two gen-
 23 erations of hematite. One population of hematite demagnetized at the highest unblock-
 24 ing temperatures and records directions that rotated along with the clasts. This com-
 25 ponent is a primary detrital remanent magnetization. The other component is removed
 26 at lower unblocking temperatures and has a consistent direction throughout the intra-
 27 clasts. This component is held by finer-grained hematite that grew and acquired a chem-
 28 ical remanent magnetization following deposition resulting in a population that includes
 29 superparamagnetic nanoparticles in addition to remanence-carrying grains. The data sup-
 30 port the interpretation that magnetizations of hematite-bearing sedimentary rocks held
 31 by >400 nm grains that unblock close to the Néel temperature are more likely to record
 32 magnetization from the time of deposition. This primary magnetization can be success-
 33 fully isolated from co-occurring authigenic hematite through high-resolution thermal de-
 34 magnetization.

35 **1 Introduction**

36 The magnetizations of hematite-bearing sedimentary rocks known as “red beds”
 37 have provided ample opportunities for Earth scientists to gain insight into the ancient
 38 geomagnetic field and the paleogeographic positions of sedimentary basins. However, with
 39 these opportunities has come much scientific debate, leading to what has been referred
 40 to as the “red bed controversy” (Beck, Burmester, & Housen, 2003; Butler, 1992; Van
 41 Der Voo & Torsvik, 2012). This controversy stems from the reality that hematite within
 42 sedimentary rocks can have two sources: 1) detrital grains that are within the sediment
 43 at the time of deposition; 2) grains that grow *in situ* after the sediments have been de-
 44 posited.

45 How does one constrain the relative age of hematite within sedimentary rocks? Many
 46 of the traditional paleomagnetic field tests are unable to differentiate between primary
 47 versus diagenetic remanence. For example, a structural fold test can constrain that a re-
 48 manence direction was obtained prior to folding, but millions of years have typically passed
 49 between the deposition of a sediment and such tectonic tilting. Dual-polarity directions
 50 through a sedimentary succession are commonly interpreted as providing assurance that
 51 the remanence records primary or near-primary magnetization; however, hematite growth
 52 could occur significantly after deposition during a protracted period over which the ge-
 53 omagnetic field was in both reversed and normal polarities. Petrographic investigations
 54 are valuable, but it can be difficult to ascertain how much the petrographically observed
 55 hematite contributes to the magnetization and to unambiguously interpret whether ob-
 56 served grains are detrital or not (e.g. Elmore & Van der Voo, 1982). A common approach
 57 to classify hematite grains within red beds is into a fine-grained pigmentary population,
 58 typically interpreted to have formed within the sediment, and a coarser-grained popu-
 59 lation that has been referred to in the literature as “specularite” (Butler, 1992; Van Der Voo
 60 & Torsvik, 2012). Tauxe, Kent, and Opdyke (1980) showed that sediments with abun-
 61 dant red pigmentary hematite in the Miocene Siwalik Group had lower thermal unblock-
 62 ing temperatures than grey samples dominated by a coarser-grained phase of specular

hematite. An additional approach taken by Tauxe et al. (1980), and other workers going back to the work of Collinson (1965), is to preferentially remove fine-grained pigmentary hematite through prolonged immersion in concentrated HCl acid. Paired chemical and thermal demagnetization have been interpreted to show that removal of pigmentary hematite coincides with removal of hematite associated with lower unblocking temperatures. These data support the interpretation that coarser grains that are more resistant to dissolution in acid correspond with those that carry remanence to the highest unblocking temperatures (Bilardello & Kodama, 2010a; Tauxe et al., 1980). Observations such as these have led to the practice of defining the characteristic remanent magnetization from hematite-bearing sediments as that held by the highest unblocking temperatures (Van Der Voo & Torsvik, 2012). Additional lines of evidence in numerous successions have supported this approach. For example, in the well-studied Carboniferous Mauch Chunk Formation of Pennsylvania, remanence removed up to \sim 660°C has uniform polarity and fails a fold test while the component removed upwards of 670°C is dual-polarity, was acquired before folding, and is interpreted as a primary magnetization (DiVenere & Opdyke, 1991; Kent & Opdyke, 1985). Nevertheless, the primary versus secondary nature of micron-scale “specularite” grains that likely carry this remanence has been one of the largest sources of contention in the “red bed controversy” (Butler, 1992; Tauxe et al., 1980; Van Der Voo & Torsvik, 2012; Van Houten, 1968).

What is needed to most confidently address the timing of remanence acquisition is a process that reorients the sediment before it has been lithified. Two such processes are: 1) syn-sedimentary slumping wherein coherent sediment is reoriented through soft-sediment folding in the surface environment and 2) intraclasts comprised of the lithology of interest that have been liberated and redeposited within the depositional environment. Sediments that have undergone reorienting processes within the depositional environment can provide significant insight into whether magnetization was acquired before or after reorientation.

Tauxe et al. (1980) studied 7 cobble-sized clasts within the Siwalik Group that were interpreted to have formed by cut-bank collapse and discovered that their magnetic remanence was acquired prior to clast reorientation. Molina-Garza, Geissman, Voo, Lucas, and Hayden (1991) observed dispersed magnetization directions in sandstone and siltstone clasts within the Triassic Moenkopi and Chinle formations in New Mexico and interpreted the characteristic remanence to be a detrital or early chemical remanence. An investigation by Purucker, Elston, and Shoemaker (1980) on red beds also of the Triassic Moenkopi Formation of Arizona used multiple such syn-sedimentary processes to gain insight into hematite acquisition. In their study, an intraformational landslide deposit with isoclinal folds of hematite-bearing claystone revealed non-uniform directions upon blanket demagnetization to 650°C that cluster better when corrected for their tilt, leading to a primary interpretation for their remanence. Scatter was also observed in intraformational conglomerate clasts weathered out of an underlying unit upon blanket thermal demagnetization to 630°C. However, the lack of principal component analysis makes it difficult to evaluate the coherency of the directions. Complicating matters, Larson and Walker (1982) analyzed shale rip-up clasts in the same Moenkopi Formation and used the fact that similar remanence directions were removed between clasts during thermal demagnetization up to 645°C as support for the hypothesis that red beds rarely reflect the geomagnetic field at the time of deposition. Evaluating the robustness of this result, as well as the varying results of similar field tests conducted by Liebes and Shive (1982) on the Chugwater and Moenkopi formations, is hindered by the cessation of thermal demagnetization before the Néel temperature of hematite and the lack of principal component analysis. These limitations are found in many studies from this era of research, when the red bed controversy was particularly fervent, as the work predates the widespread application of principal component analysis in conjunction with systematic progressive thermal demagnetization (Kirschvink, 1980; Van Der Voo & Torsvik, 2012). Using such methods, Opdyke and DiVenere (2004) analyzed 20 red siltstone rip-up clasts from the

117 Mauch Chunk Formation and found that the remanence component that unblocks above
 118 650 °C and passes a structural fold test was reoriented with the rip-up clasts providing
 119 strong evidence for a syndepositional or early post-depositional origin of the hematite.

120 In this study, we investigate cm-scale siltstone intraclasts within the ca. 1.1 Ga Freda
 121 Formation that were eroded by fluvial processes and redeposited amongst cross-stratified
 122 sandstones (Fig. 1). High-resolution thermal demagnetization data on these clasts con-
 123 strain the timing of hematite acquisition by revealing a primary component that formed
 124 prior to the erosion of the clasts within the depositional environment and a secondary
 125 component that formed following their redeposition. Rock magnetic experiments con-
 126 strain the magnetic mineralogy and provide additional insights into the grain size of the
 127 hematite populations that hold these remanences.

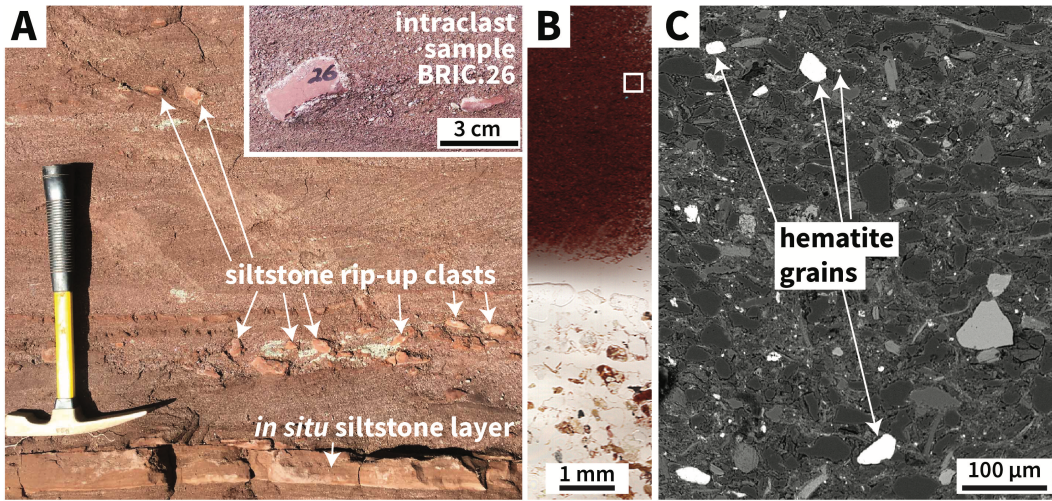


Figure 1. A: Siltstone intraclasts within the Freda Formation. The field photo shows an intact layer of siltstone below the hammer head which is topped by a bed of trough cross-stratified coarse sandstone with horizons of siltstone intraclasts. The hammer is 40 cm long. The inset photo is of an individual intraclast that was sampled as BRIC.26. B: A scan of a thin section of the BRIC.26 intraclast (upper half of image) and the coarse sand matrix (lower half of image). The red color of the intraclast is due to pigmentary hematite. C: Backscatter electron image of the siltstone clast from the region of the white box in B. The light-colored detrital grains that are labeled with arrows (light due to iron's high atomic number) were confirmed to be hematite through electron backscatter diffraction.

128 The ~5 km thick Freda Formation was deposited in the North American Midcon-
 129 tinent Rift as it was thermally subsiding following the cessation of widespread magmatic
 130 activity (Cannon, 1992). The fluvial sediments of the Freda Formation are part of the
 131 Orono Group and were conformably deposited following the deposition of the alluvial
 132 Copper Harbor Conglomerate and the lacustrine Nonesuch Formation (Ojakangas, Morey,
 133 & Green, 2001; Slotznick, Swanson-Hysell, & Sperling, 2018). Abundant fine-grained red
 134 siltstones within the Freda Formation have a well-behaved magnetic remanence domi-
 135 nated by hematite (Henry, Mauk, & Van der Voo, 1977). A maximum age constraint on
 136 the Freda Formation of $1085.57 \pm 0.25/1.3$ Ma (2σ analytical/analytical + tracer + de-
 137 cay constant uncertainty; Fairchild, Swanson-Hysell, Ramezani, Sprain, & Bowring, 2017)
 138 is provided by an U-Pb date of a lava flow within the underlying Copper Harbor Con-
 139 glomerate. Minor volcanics within the Freda Formation on the Keweenaw Peninsula are
 140 unlikely to be substantially younger than the youngest dated volcanics within the Mid-

continent basin ($1083.52 \pm 0.23/1.2$ Ma from the Michipicoten Island Formation; Fairchild et al., 2017). An age of ca. 1080 Ma for the basal 500 meters of the Freda Formation is consistent with modeling of post-rift thermal subsidence (Hutchinson, White, Cannon, & Schulz, 1990).

The studied intraclast-bearing outcrop is located along the Bad River (northern Wisconsin) in the lower portion of the Freda Formation – approximately 320 to 340 meters above its conformable base with the Nonesuch Formation (latitude: 46.3866° N, longitude 90.6373° W). The two main lithofacies in the studied outcrop are: (1) siltstone to very fine sandstone with planar lamination and horizons of ripple cross-stratification and (2) coarse to very coarse subarkosic sandstone with dune-scale trough cross-stratification (Fig. 1). These lithofacies are consistent with a fluvial depositional environment where the coarse sandstone facies are channel deposits and the siltstones are inner-bank or overbank deposits. The coarse-grained sandstone contains horizons of tabular cm-scale intraclasts comprised of the red siltstone lithology that is present in underlying beds of intact siltstone (Fig. 1). These tabular clayey-silt intraclasts were eroded within the depositional environment and redeposited in the sandstone. Due to migrating channels in fluvial systems, it is expected that a river will erode its own sediments. The intraclasts would have been held together through cohesion resulting from the clay component within the sediment. Given that the clasts are large (1 to 7 cm) relative to their host sediment, that they are angular, and that they would have been fragile at the time of deposition, it is unlikely that they were transported far within the channel.

Paleomagnetic Results

Oriented samples were collected and analyzed from 39 Freda Formation intraclasts. The dimensions of the sampled clasts ranged from $2.2 \times 1.4 \times 0.5$ cm to $7.2 \times 2.3 \times 1.2$ cm. Given that the clasts were typically smaller than the 1-inch-diameter drill cores used for sampling, they were collected along with their sandstone matrix. These oriented cores were mounted onto quartz glass discs with Omega CC cement and the matrix material was micro-drilled away. The mounted clasts underwent stepwise thermal demagnetization in the UC Berkeley Paleomagnetism Lab using an ASC demagnetizer (residual fields <10 nT) with measurements made on a 2G DC-SQUID magnetometer. The demagnetization protocol had high resolution approaching the Neél temperature of hematite (5°C to 2°C to 1°C) resulting in 30 total thermal demagnetization steps (Fig. 2). All paleomagnetic data are available to the measurement level in the MagIC database (<https://earthref.org/MagIC/doi/>). So that reviewers have access to the data, they are currently available in CIT lab format and MagIC format here: https://github.com/Swanson-Hysell-Group/2018_Red_Bed_Intraclasts.

The clasts typically reveal two distinct magnetization directions. One direction was similar throughout the intraclasts and was typically removed between 200°C and 650°C (Fig. 2). This mid-temperature component is continuously unblocked between these temperatures with no or minimal downward inflection at $\sim 580^{\circ}\text{C}$ that would indicate appreciable remanence associated with magnetite (Fig. 2). This component is directionally well-grouped indicating that it was acquired following deposition of the clasts (Fig. 2). The other component trends towards the origin and is removed by thermal demagnetization steps at the highest levels such that it typically can be fit by a least-squares line between 665°C and 688°C . The relative magnitude of the components varies between intraclasts (Fig. 2). While the high-temperature component can sometimes be fit as a line with a lower temperature bound of 660°C (BRIC.31a in Fig. 2), due to overlapping unblocking temperatures between the mid-temperature and high-temperature components, the lower bounds of the high-temperature fits sometimes need to be as high as 680°C (BRIC.41a in Fig. 2). Note that while the Neél temperature of hematite is sometimes given as 675°C in the paleomagnetic literature, experimental data often show the Neél temperature to be as high as 690°C (Özdemir & Dunlop, 2006). In the data from the clasts,

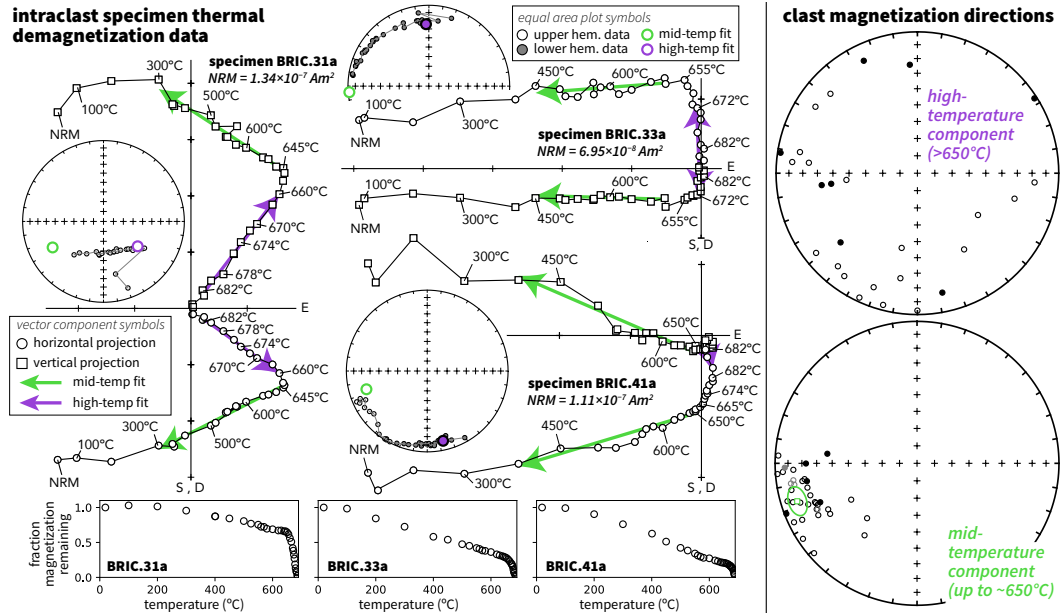


Figure 2. Paleomagnetic data from intraclasts reveal a mid-temperature component that typically unblocks prior to 655°C and a high-temperature component that typically unblocks between 655°C and 687°C. These components are present as varying fractions of the overall remanence as seen in the three individual clasts shown here on vector component plots and measurement-level equal area plots in tilt-corrected coordinates (developed using PmagPy; Tauxe et al., 2016). The direction of the mid-temperature component is shown as green arrows on the vector component plots and green circles on the equal area plots while the high-temperature component is shown with purple symbols. The mid-temperature component has a similar direction among the clasts as can be seen on the component directions equal area plots (tilt-corrected mean declination: 252.4, inclination: -12.5, α_{95} : 6.6). In contrast, the high-temperature component directions are dispersed.

there is typically a significant directional change in the specimen magnetization between the mid-temperature component and the high-temperature component (Fig. 2). As a result, 29 of the 39 analyzed intraclast specimens could be fit with distinct mid-temperature and high-temperature least-squares lines. An additional five specimens were undergoing directional change through the highest thermal demagnetization steps indicative of the presence of a distinct high-temperature component, but this component was not well-expressed enough to be fit. Five of the specimens showed no directional change and could be fit with a single mid-to-high-temperature component that is grouped with the mid-temperature component directions. In contrast to the well-grouped mid-temperature component, the high-temperature component directions are dispersed, indicating that the component was acquired prior to erosion and redeposition of the clasts. The high-temperature component directions are more dispersed in declination than inclination leading to a distribution that is not randomly dispersed on a sphere. Given that the clasts are tabular, were liberated along their depositional lamination, and subsequently landed roughly bedding-parallel, it is to be expected that the rotations were largely around a vertical axis – preferentially changing declination.

In-place siltstone and very fine sandstone, representing the same lithologies that were liberated into intraclasts, were collected and analyzed following the same thermal demagnetization protocol. These samples were collected from a section stratigraphically

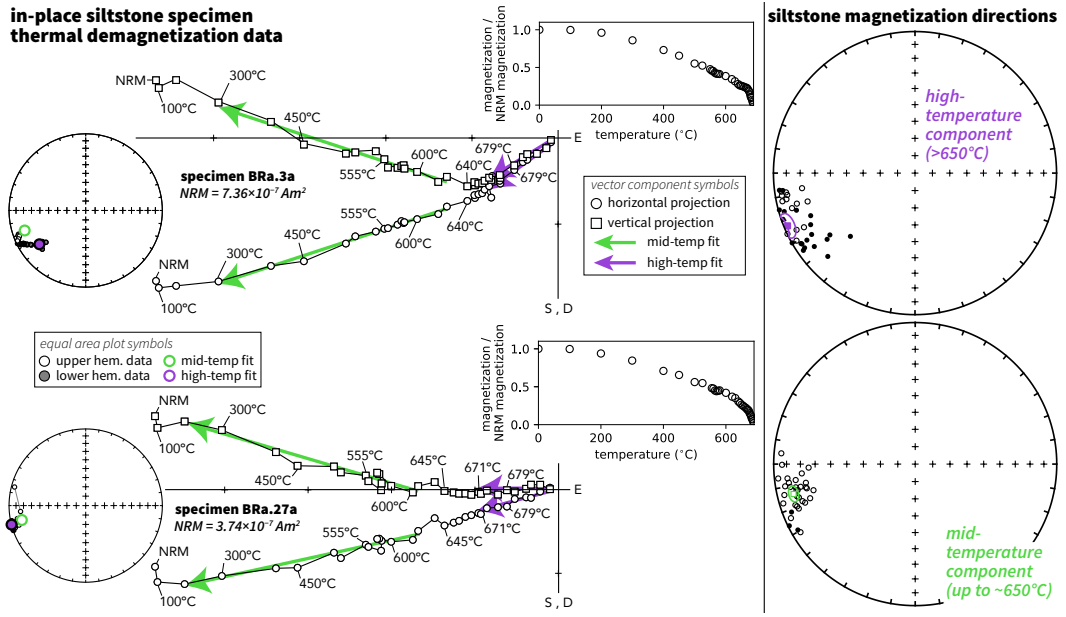


Figure 3. Paleomagnetic data from in-place siltstone beds reveal a mid-temperature component that typically unblocks prior to 655°C and a high-temperature component that typically unblocks between 655°C and 689°C. The direction of the mid-temperature component is shown as purple arrows on the vector component plots and purple circles on the equal area plots while the high-temperature component is shown with green symbols. The mid-temperature component is similar to that removed from the clasts. The high-temperature component is well-grouped and has a distinct direction from the mid-temperature component with lower inclination.

below the intraclast-bearing outcrop along a small tributary creek to the Bad River (section BRa; latitude: 46.3852 °N, longitude 90.6337 °W). These samples are between 50 and 70 meters above the base of the Freda Formation. The thermally demagnetized specimens display very similar demagnetization behavior to the intraclasts with a mid-temperature component that progressively unblocks up to ~650 °C and then transitions to a slightly different direction that unblocks up to ~689 °C. The mid-temperature component (tilt-corrected Dec = 256.2, Inc = -12.5, $\alpha_{95} = 3.6$) shares a common mean with the mid-temperature component isolated from the intraclast samples (tilt-corrected Dec = 252.4, Inc = -12.5, $\alpha_{95} = 6.6$). The high-temperature component directions are well-grouped, in contrast to their dispersion between the intraclasts, and have a direction that is similar, but distinct, from the mid-temperature component (i.e. the two means can be distinguished at the 95% confidence level). The inclination of the high-temperature component mean is very close to horizontal (Fig. 3; tilt-corrected Dec = 247.5, Inc = 3.0, $\alpha_{95} = 5.4$).

The paleomagnetic results on the in-place siltstone beds are similar to those obtained by Henry et al. (1977) who studied the basal Freda Formation in the Presque Isle Syncline and White Pine Basin of northern Michigan. As in our results, their data revealed a distinct mid-temperature component with a shallow upwards inclination and a high-temperature component with a near horizontal inclination. A progression from horizontal to upward inclinations is consistent with the expected change through time if the movement along the Keweenawan Track persisted past the end of rift magmatism (Fairchild et al., 2017; Swanson-Hysell, Ramezani, Fairchild, & Rose, 2018) and is consistent with a later age of remanence acquisition for the mid-temperature component. While the inclination of the mid- and high-temperature components are indistinguish-

able between our data and that of Henry et al. (1977), the declinations are different such that their declinations are 24° more northerly than those obtained for BRa. The origin of this difference in declination is unclear and could be associated with complications in the tilt-correction such as non-cylindrical folding or multiple tilting episodes (inclination is relative to bedding tilt so would not be effected by such processes). It is premature to recalculate a paleomagnetic pole for the Freda Formation. More analyses are needed from the Freda Formation: 1) to evaluate this declination discrepancy; 2) develop enough directional data to robustly apply the elongation/inclination method for inclination flattening correction (>100 to 150 samples necessary per Tauxe, Kodama, & Kent, 2008) to increase the quality of the paleomagnetic pole for the purposes of paleogeographic reconstruction and 3) expand data to span the stratigraphic thickness of the formation as current results are limited to the basal portion of the formation.

247 Petrographic Results

248 Petrography on the intraclasts reveals two distinct populations of hematite (Fig. 1). One population is fine-grained pigmentary hematite present dominantly within the
 249 clay-sized matrix and rimming detrital silt-sized grains. The zones of pigmentary hematite
 250 within the matrix remain cloudy to high magnification indicating that the grains are sub-
 251 micron in size. The other population of hematite has similar sizes and shapes to other
 252 detrital silt-sized grains – typically ranging from 2 to 50 μm in diameter. These hematite
 253 grains were identified through reflected light microscopy with their mineralogy supported
 254 by energy-dispersive x-ray spectroscopy conducted on a scanning electron microscope
 255 (SEM) at Lawrence Berkeley National Laboratory and confirmed by electron backscat-
 256 ter diffraction on an SEM at UC Berkeley (see Supporting Information).

258 Rock Magnetic and Mössbauer Spectroscopy Results

259 The paleomagnetic data reveal that there are two distinct populations of remanence-
 260 carrying magnetic grains within the intraclasts and in-place siltstone with differing un-
 261 blocking temperature ranges: one unblocking over a broad temperature range from 100
 262 $^{\circ}\text{C}$ up to 650 $^{\circ}\text{C}$ or higher and the other dominantly unblocking between 665 $^{\circ}\text{C}$ and 690 $^{\circ}\text{C}$.
 263 Rock magnetic experiments and Mössbauer spectroscopy can elucidate additional prop-
 264 erties associated with the ferromagnetic mineralogy within the siltstone that is carry-
 265 ing the remanence as well as portions of the magnetic mineralogy that are not stable at
 266 room temperature.

267 Backfield demagnetization curves, where the specimens were saturated in a 1.8 T
 268 field followed by a progressively larger field in the opposite direction, were developed on
 269 a Princeton Measurements vibrating sample magnetometer at the Institute for Rock Mag-
 270 netism. Coercivity spectra, the derivative of the backfield curves, were modeled using
 271 the Max UnMix software package (Maxbauer et al., 2016; Fig. 4). These spectra are well
 272 fit with two log-normal distributions associated with two populations of grains. One pop-
 273 ulation has a median coercivity of ~ 300 mT and a distribution that extends from the
 274 lowest to the highest coercivities (Fig. 4). The other population has a higher median co-
 275 ercivity of ~ 700 mT and a coercivity distribution that is limited to the high coercivity
 276 range (Fig. 4). The median coercivity of the high-coercivity phase corresponds well with
 277 the coercivity of single-domain hematite in the 300 nm to 10 μm range (Özdemir & Dun-
 278 lop, 2014). The spread in coercivities associated with the lower coercivity population is
 279 consistent with these values down to those associated with finer-grained hematite; the
 280 coercivity of hematite becomes progressively lower for grains that are smaller than 300
 281 nm in diameter (Özdemir & Dunlop, 2014).

282 The frequency and temperature dependence of magnetic susceptibility was deter-
 283 mined through experiments conducted on a Magnetic Properties Measurement System
 284 (MPMS) at the Institute for Rock Magnetism. The dependence of susceptibility on both

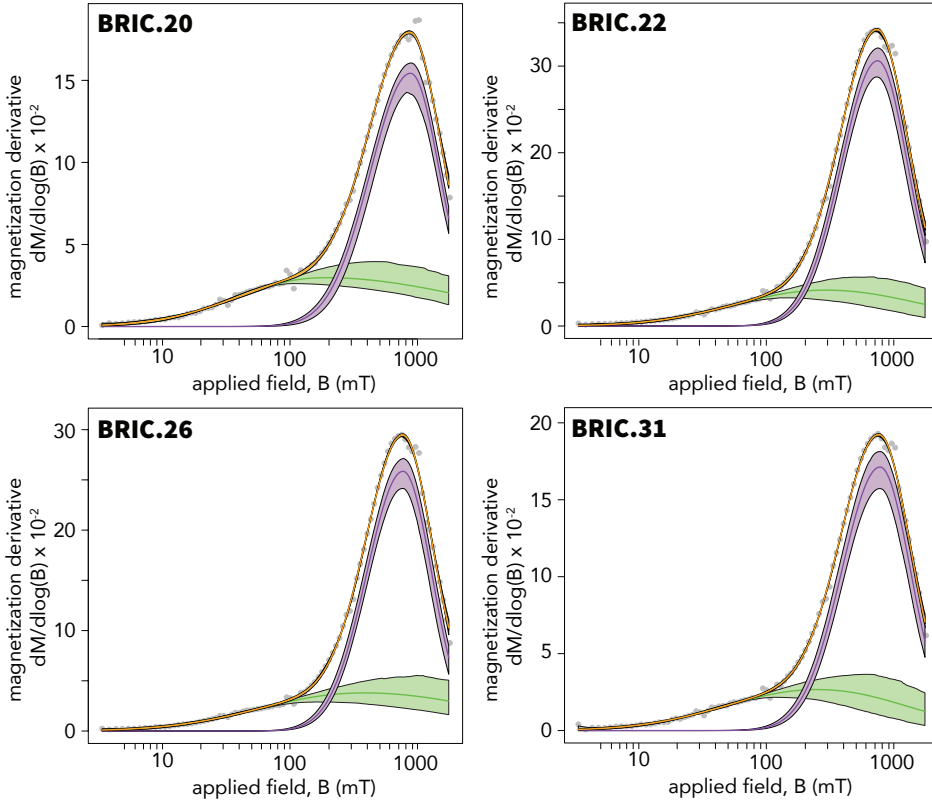


Figure 4. Coercivity spectra developed from backfield demagnetization curves on BRIC intraclast specimens with the points being the data. The data were modeled using log-Gaussian functions implemented with the Max UnMix software package (Maxbauer et al., 2016) with the yellow curve corresponding to the model. The coercivity spectra can be well-explained with two distributions: the higher coercivity distribution in purple and the lower coercivity distribution in green.

temperature and frequency provides a sensitive and diagnostic means of characterizing magnetic nanoparticles (Worm & Jackson, 1999). We observe a frequency dependence of susceptibility that persists from 300 K down to 10 K (Fig. 5). This frequency dependence can be attributed to viscous superparamagnetic grains whose magnetic viscosity has relaxation times comparable to the AC field reversal interval (Worm, 1998; Worm & Jackson, 1999). This interpretation is supported by the frequency dependence of the in-phase susceptibility and the shared peak between the out-of-phase (quadrature) susceptibility and the $\pi/2$ law (Mullins & Tite, 1973; Fig. 5). That the frequency dependence extends across the full low-temperature range indicates a broad blocking temperature spectrum of viscous superparamagnetic grains associated with a wide size distribution of the nanoparticles.

Hysteresis loops were measured from 5 T to -5 T on the MPMS at varying temperatures from room temperature (300 K) down to 50 K (Fig. 6). These low-temperature hysteresis data reveal a progressive increase in remanent magnetization (M_r) as temperature decreases (Fig. 6) leading to M_r values that are between 9 and 13% higher at 50 K than at 300 K. This increase in M_r at low temperatures is likely associated with superparamagnetic grains transitioning to behave as stable single domain grains at lower temperature. There is also an increase in saturation magnetization (M_s) as temperature

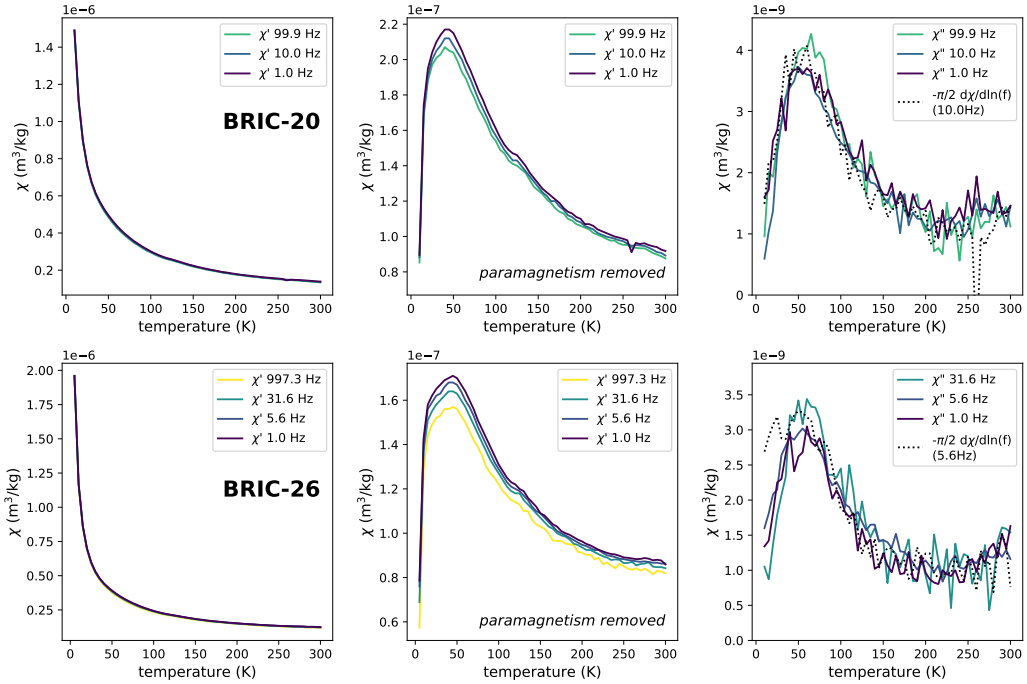


Figure 5. Frequency and temperature dependence of magnetic susceptibility (χ) for BRIC-20 and BRIC-26 from 10 to 300 K. The left panels show the in-phase susceptibility which is dominated by the paramagnetic component of the samples. In the middle panels, this paramagnetic component has been removed by creating a Curie-Weiss law model and subtracting it from the in-phase susceptibility data. Strong frequency dependence over the whole temperature range suggests a broad size distribution of nanoparticles (e.g. Jackson & Swanson-Hysell, 2012). The right panels show the out-of-phase (quadrature) susceptibility as well as the $\pi/2$ relationship of χ'' [viscosity] = $-(\pi/2)(\partial\chi'/\partial\ln(f))$ where f =frequency. These data document the presence of viscous superparamagnetic particles.

decreases (Fig. 6). However, the hysteresis loops require subtraction of a large paramagnetic component that becomes progressively non-linear at low temperatures leading to the possibility that this increase in M_s is an artefact rather than an aspect of the ferromagnetic mineralogy of the samples. This increase in M_r is insensitive to this correction and is therefore a more robust feature of the data.

Mössbauer spectra were collected at the Institute for Rock Magnetism on bulk powders of intraclast samples at 300 K and 18 K (Fig. 7). The main feature of these spectra is a magnetically split sextet with a magnetic hyperfine field of about 51.6 T – diagnostic of hematite (Dyar, Agresti, Schaefer, Grant, & Sklute, 2006). Modeling of the spectra reveal that the majority of iron within the samples resides within hematite (58% at 300 K and 60% at 18 K). Due to the high-frequency of Mössbauer spectroscopy, grains that are observed to be superparamagnetic at room temperature in typical rock magnetic experiments behave as stable ordered grains in Mössbauer spectra. Nevertheless, there is a slight increase in the magnitude of the hematite sextet relative to the doublets in the 18 K spectrum, leading to the slight increase in modeled hematite content, likely associated with ordering of the smallest nanoparticles of hematite (Bødker, Hansen, Koch, Lefmann, & Mørup, 2000; Fig. 7).

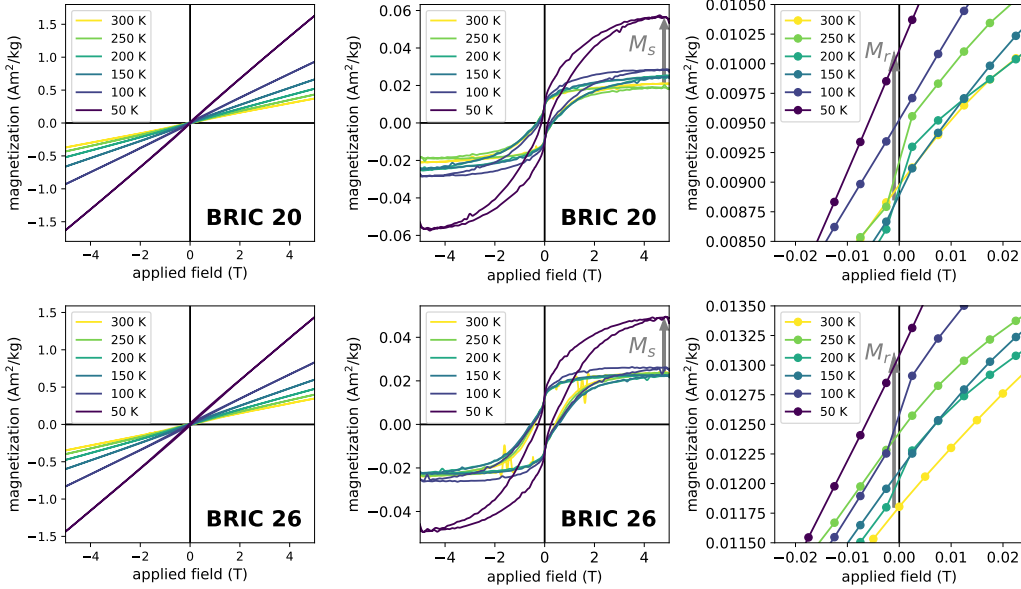


Figure 6. Hysteresis loops measured from room temperature (300 K) down to 50 K for silt-stone intraclast samples. The left panels are the raw uncorrected loops, the center panels remove the paramagnetic contribution using the methods of Jackson and Solheid (2010) and the right panels zoom-in on applied fields close to 0 to illustrate the progressive increase in remanent magnetization (M_r) as temperature decreases.

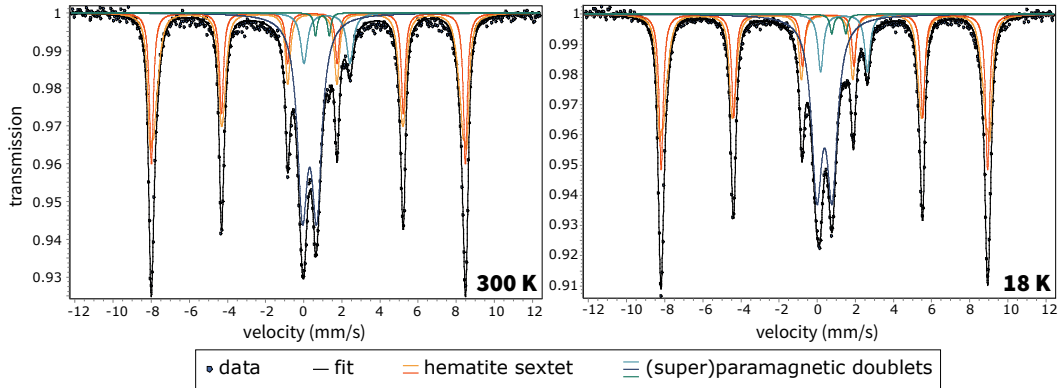


Figure 7. Mössbauer spectra developed at room temperature (300 K) and low temperature (18 K) on a powder of intraclast sample BRIC.22. Data are shown as dots with the black line representing a model fit. The sextet portion of the fit is shown with the red and yellow curves (representing the spread in hyperfine splitting resulting from a natural population) and is diagnostic of hematite. The central peak is comprised of doublets dominated by Fe^{3+} . The height of the hematite sextet relative to the central peak is slightly higher in the low temperature experiment likely due to ordering of the smallest hematite nanoparticles.

DISCUSSION

Single-domain hematite grains have high coercivities (>150 mT; Özdemir & Dunlop, 2014) and high unblocking temperatures. As a result, populations of hematite within

rocks are stable on long timescales, resistant to overprinting, and therefore attractive for paleomagnetic study. In contrast to magnetite, hematite grains retain stable single-domain behavior in crystals $>1\ \mu\text{m}$ with the threshold to multidomain behavior occurring when grain diameters exceed $\sim 100\ \mu\text{m}$ (Kletetschka & Wasilewski, 2002; Özdemir & Dunlop, 2014). Hematite nanoparticles with diameters $<30\ \text{nm}$ have superparamagnetic behavior wherein thermal fluctuation energy overwhelms the ability of the grain to retain a stable magnetization at Earth surface temperatures (Özdemir & Dunlop, 2014). Hematite grains become progressively less influenced by thermal fluctuations as they reach grain sizes of a few hundred nanometers at which point they are stable up to temperatures approaching the Néel temperature of $\sim 685^\circ\text{C}$ (Özdemir & Dunlop, 2014; Swanson-Hysell, Feinberg, Berquó, & Maloof, 2011). As a result, there is a strong relationship between grain volume and unblocking temperature that can be utilized to estimate grain size following Néel relaxation theory (Néel, 1949; Swanson-Hysell et al., 2011). A hematite population that is progressively unblocking at thermal demagnetization steps well below the Néel transition temperature, such as the mid-temperature component of the intraclasts, is comprised of grains within the ~ 30 to $\sim 400\ \text{nm}$ size range (Fig. 8). This fine-grain size is consistent with the pigmentary phase observed within the intraclasts (Fig. 1).

Given the directional consistency of the mid-temperature component among the intraclasts (Fig. 2), this component must have dominantly formed as a chemical remanent magnetization after the intraclasts were redeposited in the channel. Chemical remanent magnetization acquisition by pigmentary hematite would have occurred as hematite grains grew to sizes above the superparamagnetic to stable single-domain transition resulting in the wide range of unblocking temperatures that is observed. The frequency dependence of susceptibility (Fig. 5) and increase in remanent magnetization following saturation at low-temperature (Fig. 6) both indicate the presence of a population of superparamagnetic grains. The coercivity spectra are consistent with a population of hematite that has a wide coercivity range extending from low coercivities up to high coercivities (the green component in the unmixing models of Fig. 4). Taken together and compared to the hematite coercivity compilation of Özdemir and Dunlop (2014), these data indicate that a population of authigenic hematite nanoparticles that spans from $<30\ \text{nm}$ to $>300\ \text{nm}$ is responsible for the post-depositional chemical remanent magnetization (Fig. 8).

In contrast, the sharp unblocking temperature close to the Néel temperature of the high-temperature component indicates that it is dominantly held by hematite grains that are $>400\ \text{nm}$ (based on Néel relaxation theory; Fig. 8) such as the silt-sized hematite grains observed petrographically (Fig. 1). The high-coercivity population within the coercivity spectra (purple curves in Fig. 4) are consistent with this grain-size interpretation (Fig. 8). The high-temperature remanence component held by these grains was rotated along with the clasts indicating that it is primary and was acquired prior to the redeposition of the cohesive silt clasts. That this component is held by larger grain sizes supports it being a detrital remanent magnetization, rather than a chemical remanent magnetization that formed very early prior to clast erosion.

Detailed rock magnetic data through the Nonesuch Formation, which immediately underlies the Freda Formation, reveal that the lacustrine lithologies preserve a depth-dependent environmental magnetic signature where the deep water facies have no hematite in contrast to hematite-rich shallow water facies in sediments of similar grain size (Slotznick et al., 2018). This difference was interpreted by Slotznick et al. (2018) as being due to microbial reductive dissolution of iron oxides at low oxygen levels in the deepest part of the lake and oxidation of the detrital input in the shallowest part of the lake. That this depth-dependent relationship is consistent over significant length scales across the Mid-continent Rift basin indicates that hematite formation in those sediments, and likely the Freda Formation as well, is associated with redox conditions at the time of deposition rather than the subsequent migration of fluids. Oxidation of iron in surface environments

often begins with the formation of fine-grained poorly crystalline ferrihydrite, which transforms to stable crystalline hematite at neutral pH on geologically short timescales (Cudennec & Lecerf, 2006; Jiang et al., 2018). The broad unblocking temperatures we observe for the chemical remanent magnetization in the Freda intraclasts are similar to those in hematite populations produced through experimental ferrihydrite to hematite conversion (Jiang et al., 2015). The direction of this chemical remanence is distinct, but similar, to that of the detrital remanence with a change in both declination and inclination. This result suggests that the chemical remanence was acquired as plate motion continued at the end of the Keweenawan Track (Swanson-Hysell et al., 2018). This chemical remanent magnetization direction is well-grouped (Fig. 3) suggesting that the hematite that carries the remanence formed at a similar time rather than over a protracted period (which could lead to a streaked distribution; Beck et al., 2003). One possibility is that the conversion from a phase associated with the ferrihydrite to hematite transition that formed in the sediments in the near-surface was thermally activated by the geothermal gradient as the sediments were buried. More than 4 km of Freda Formation sediments were deposited atop those investigated in this study within the thermally subsiding basin that would have led to protracted interval at temperatures >100 °C following deposition. Such thermal activation of the transition of ferrihydrite, and/or intermediary phases such as hydromaghemite, to hematite could explain the association of chemical remanence directions with burial within the Midcontinent Rift. This mechanism could also explain the association of authigenic hematite remanence with other types of tectonothermal events such as the well-documented syn-folding chemical remanence of the Mauch Chunk Formation that is associated with the Alleghanian orogeny (Kent & Opdyke, 1985; Opdyke & DiVenere, 2004).

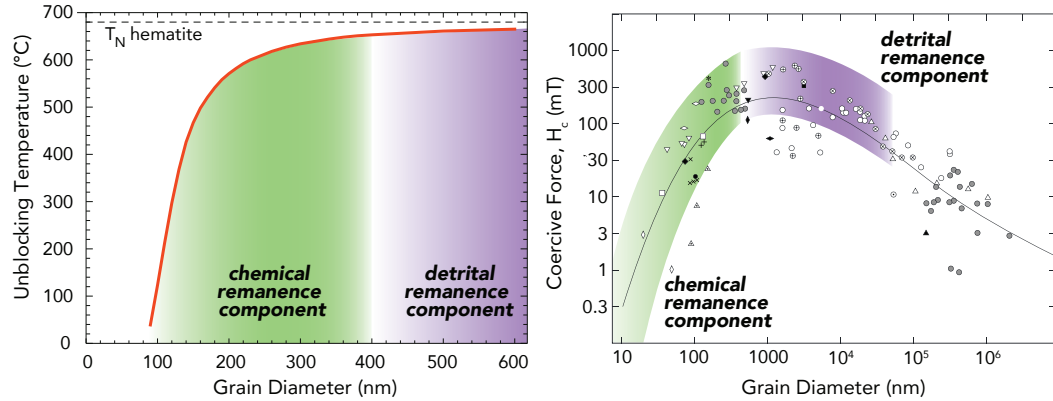


Figure 8. Left: Calculated unblocking temperatures using Néel thermal relaxation theory of idealized spherical hematite grains using a thermal fluctuation rate of 10^{10} s⁻¹ and a relaxation time of 5 minutes for comparison to thermal demagnetization data (modified from Swanson-Hysell et al., 2011). The unblocking temperatures of the mid-temperature chemical component (green) and the high-temperature detrital component (purple) are shown and can be used to infer grain size. The Néel transition temperature (T_N) is shown with a dashed line. Right: Compilation of coercivity data from hematite as a function of grain diameter from Özdemir and Dunlop (2014). The higher coercivity population from Fig. 4 corresponds to the larger grain sizes than the lower coercivity component associated with the chemical remanence.

The differential unblocking temperature spectra of the two components within the Freda intraclasts provides strong support for the argument of Jiang et al. (2015) that chemical and detrital remanent magnetization can be distinguished due to detrital remanence unblocking at the highest temperatures. However, the Freda intraclast data also

404 show that while the detrital remanent magnetization can be well-isolated at tempera-
 405 tures as low as 650°C (specimen BRIC.31a in Fig. 2), the chemical remanent magneti-
 406 zation thermal unblocking spectra can overlap with that of the detrital remanence and
 407 extend up to temperatures closer to the Néel temperature (specimen BRIC.41a in Fig.
 408 2). Therefore, to isolate primary remanence in red beds, best practice should be to pro-
 409 ceed with very high resolution thermal demagnetization steps above 600°C, and partic-
 410 ularly above 650°C. Characteristic remanence magnetization directions associated with
 411 hematite that are fit to components that span a wide range of unblocking temperatures
 412 including those lower than ~650 °C are likely convolving a pigmentary chemical rema-
 413 nance and a detrital remanence held by larger grains.

414 A complication with detrital remanent magnetization is associated inclination-shallowing
 415 – an issue that has been explored in depth within the literature as pertains to hematite
 416 (e.g Bilardello & Kodama, 2010b; Tauxe & Kent, 1984). The presence of both pigmen-
 417 tary and detrital hematite complicates efforts that seek to use bulk magnetic fabrics to
 418 correct for these effects. This reality necessitates the use of careful methodologies that
 419 target the fabric of only the highest-unblocking-temperature hematite (e.g. Bilardello,
 420 2015) or that take other approaches such as analyzing the elongation of the directional
 421 distribution and correcting to values taken from secular variation models (the elongation-
 422 inclination method of Tauxe & Kent, 2004).

423 Hematite-bearing sedimentary rocks have varied characteristics which has lead to
 424 the argument that it is difficult to apply results from red beds in one formation to those
 425 from another. However, the rock magnetic properties of the hematite grain size distri-
 426 butions that emerge from these data are associated with their mode of incorporation into
 427 the sediment. Hydrodynamic sorting associated with the delivery of detrital hematite
 428 will lead to a narrower and coarser size distribution of grains than that of authigenic pig-
 429 mentary hematite growth. Authigenic growth can lead to a distribution of grains that
 430 span from sub-30 nm superparamagnetic grains up to stable single-domain grains >300
 431 nm in diameter. Such an authigenic population has distinct rock magnetic charac-
 432 teristics including a very broad coercivity distribution and viscous superparamagnetic grains
 433 that can be detected through low-temperature magnetometry.

434 Overall, the intraclast data, combined with those of the in-place siltstone, reveal
 435 that directional change at the highest unblocking temperatures provides an effective means
 436 to discriminate primary and secondary magnetizations within siltstones of the Freda For-
 437 mation. The isolation of remanence carried by primary detrital hematite in >1 billion-
 438 year-old siltstones lends confidence to magnetostratigraphic records and paleogeographic
 439 interpretations that are based on interpretations of primary magnetization isolated from
 440 high-unblocking-temperature hematite in ancient red beds.

441 Acknowledgments

442 This research was supported by the Esper S. Larsen, Jr. Research Fund and the National
 443 Science Foundation through grant EAR-1419894. Rock magnetic experiments were con-
 444 ducted on a visiting fellowship at the Institute for Rock Magnetism which is made pos-
 445 sible through the Instrumentation and Facilities program of the National Science Foun-
 446 dation, Earth Science Division and funding from the University of Minnesota. SPS was
 447 supported by the Miller Institute for Basic Research in Science. The Wisconsin Depart-
 448 ment of Natural Resources granted a research and collection permit that enabled sam-
 449 pling within Copper Falls State Park. Oliver Abbott assisted with field work, Taiyi Wang
 450 assisted with paleomagnetic analyses and Tim Teague provided technical support for EBSD
 451 analyses. Peat Solheid, Mike Jackson, and Dario Bilardello provided technical support
 452 at the Institute for Rock Magnetism. Discussions with them, and with Josh Feinberg and
 453 Bruce Moskowitz, provided insight on rock magnetic data interpretation. Data associ-
 454 ated with this study are available within the MagIC database and a Github repository
 455 associated with this work.

456 **References**

- 457 Beck, M. E., Burmester, R. F., & Housen, B. A. (2003). The red bed contro-
 458 versy revisited: shape analysis of Colorado Plateau units suggests long
 459 magnetization times. *Tectonophysics*, *362*(1-4), 335–344. doi: 10.1016/
 460 s0040-1951(02)00644-3
- 461 Bilardello, D. (2015). Isolating the anisotropy of the characteristic remanence-
 462 carrying hematite grains: a first multispecimen approach. *Geophysical Journal
 463 International*, *202*(2), 695–712. doi: 10.1093/gji/ggv171
- 464 Bilardello, D., & Kodama, K. P. (2010a). Palaeomagnetism and magnetic anisotropy
 465 of Carboniferous red beds from the Maritime Provinces of Canada: evidence
 466 for shallow palaeomagnetic inclinations and implications for North American
 467 apparent polar wander. *Geophysical Journal International*, *180*(3), 1013–1029.
 468 doi: 10.1111/j.1365-246x.2009.04457.x
- 469 Bilardello, D., & Kodama, K. P. (2010b). Rock magnetic evidence for inclination
 470 shallowing in the early Carboniferous Deer Lake Group red beds of western
 471 Newfoundland. *Geophysical Journal International*, *181*(1), 275–289. doi:
 472 10.1111/j.1365-246x.2010.04537.x
- 473 Bødker, F., Hansen, M. F., Koch, C. B., Lefmann, K., & Mørup, S. (2000). Mag-
 474 netic properties of hematite nanoparticles. *Physical Review B*, *61*(10), 6826–
 475 6838. doi: 10.1103/physrevb.61.6826
- 476 Butler, R. (1992). *Paleomagnetism: Magnetic domains to geologic terranes*. Black-
 477 well Scientific Publications.
- 478 Cannon, W. F. (1992). The Midcontinent rift in the Lake Superior region with em-
 479 phasis on its geodynamic evolution. *Tectonophysics*, *213*(1-2), 41–48. doi: 10
 480 .1016/0040-1951(92)90250-A
- 481 Collinson, D. W. (1965). Origin of remanent magnetization and initial susceptibility
 482 of certain red sandstones. *Geophysical Journal International*, *9*(2-3), 203–217.
 483 doi: 10.1111/j.1365-246x.1965.tb02071.x
- 484 Cudennec, Y., & Lecerf, A. (2006). The transformation of ferrihydrite into goethite
 485 or hematite, revisited. *Journal of Solid State Chemistry*, *179*(3), 716–722. doi:
 486 10.1016/j.jssc.2005.11.030
- 487 DiVenere, V. J., & Opdyke, N. D. (1991). Magnetic polarity stratigraphy in the up-
 488 permost Mississippian Mauch Chunk Formation, Pottsville, Pennsylvania. *Ge-
 489 ology*, *19*(2), 127. doi: 10.1130/0091-7613(1991)019<0127:mpsitu>2.3.co;2
- 490 Dyar, M. D., Agresti, D. G., Schaefer, M. W., Grant, C. A., & Sklute, E. C. (2006).
 491 Mössbauer spectroscopy of earth and planetary materials. *Annual Review of
 492 Earth and Planetary Sciences*, *34*(1), 83–125. doi: 10.1146/annurev.earth.34
 493 .031405.125049
- 494 Elmore, R. D., & Van der Voo, R. (1982). Origin of hematite and its associated re-
 495 manence in the Copper Harbor Conglomerate (Keweenawan), upper Michigan.
 496 *J. Geophys. Res.*, *87*(B13), 10918–10928. doi: 10.1029/JB087iB13p10918
- 497 Fairchild, L. M., Swanson-Hysell, N. L., Ramezani, J., Sprain, C. J., & Bowring,
 498 S. A. (2017). The end of Midcontinent Rift magmatism and the paleogeogra-
 499 phy of Laurentia. *Lithosphere*, *9*(1), 117–133. doi: 10.1130/L580.1
- 500 Henry, S., Mauk, F., & Van der Voo, R. (1977). Paleomagnetism of the upper Ke-
 501 weenawan sediments: Nonesuch Shale and Freda Sandstone. *Canadian Journal
 502 of Earth Science*, *14*, 1128–1138. doi: 10.1139/e77-103
- 503 Hutchinson, D., White, R., Cannon, W., & Schulz, K. (1990). Keweenaw hot spot:
 504 Geophysical evidence for a 1.1 Ga mantle plume beneath the Midcontinent
 505 Rift System. *Journal of Geophysical Research: Solid Earth*, *95*(B7), 10869–
 506 10884. doi: 10.1029/jb095ib07p10869
- 507 Jackson, M., & Solheid, P. (2010). On the quantitative analysis and evaluation of
 508 magnetic hysteresis data. *Geochem. Geophys. Geosyst.*, *11*(4). doi: 10.1029/
 509 2009GC002932
- 510 Jackson, M., & Swanson-Hysell, N. (2012). Rock magnetism of remagnetized car-

- 511 bonate rocks: Another look. In R. Elmore (Ed.), *Remagnetization and chemical alteration of sedimentary rocks* (Vol. 371). Geological Society London, Special Publications. doi: 10.1144/SP371.3
- 512 Jiang, Z., Liu, Q., Dekkers, M. J., Tauxe, L., Qin, H., Barrón, V., & Torrent, J.
 513 (2015, Oct). Acquisition of chemical remanent magnetization during experimental ferrihydrite–hematite conversion in earth-like magnetic field—
 514 implications for paleomagnetic studies of red beds. *Earth and Planetary Science Letters*, 428, 1–10. doi: 10.1016/j.epsl.2015.07.024
- 515 Jiang, Z., Liu, Q., Roberts, A. P., Barrón, V., Torrent, J., & Zhang, Q. (2018).
 516 A new model for transformation of ferrihydrite to hematite in soils and
 517 sediments. *Geology*. Retrieved from <http://10.1130/G45386.1> doi:
 518 10.1130/g45386.1
- 519 Kent, D. V., & Opdyke, N. D. (1985). Multicomponent magnetizations from the
 520 mississippian mauch chunk formation of the central appalachians and their
 521 tectonic implications. *Journal of Geophysical Research: Solid Earth*, 90(B7),
 522 5371–5383. doi: 10.1029/jb090ib07p05371
- 523 Kirschvink, J. (1980). The least-squares line and plane and the analysis of paleomagnetic data. *Geophysical Journal of the Royal Astronomical Society*, 62(3), 699–
 524 718. doi: 10.1111/j.1365-246x.1980.tb02601.x
- 525 Kletetschka, G., & Wasilewski, P. J. (2002). Grain size limit for SD hematite.
 526 *Physics of the Earth and Planetary Interiors*, 129, 173–179. doi: 10.1016/S0031-9201(01)00271-0
- 527 Larson, E. E., & Walker, T. R. (1982, Jun). A rock magnetic study of the lower
 528 massive sandstone, Moenkopi Formation (Triassic), Gray Mountain Area, Arizona.
 529 *Journal of Geophysical Research: Solid Earth*, 87(B6), 4819–4836. doi:
 530 10.1029/jb087ib06p04819
- 531 Liebes, E., & Shive, P. N. (1982, Dec). Magnetization acquisition in two Mesozoic
 532 red sandstones. *Physics of the Earth and Planetary Interiors*, 30(4), 396–404.
 533 Retrieved from [http://dx.doi.org/10.1016/0031-9201\(82\)90049-8](http://dx.doi.org/10.1016/0031-9201(82)90049-8) doi: 10
 534 .1016/0031-9201(82)90049-8
- 535 Maxbauer, D. P., Feinberg, J. M., & Fox, D. L. (2016, Oct). MAX UnMix: A web
 536 application for unmixing magnetic coercivity distributions. *Computers and
 537 Geosciences*, 95, 140–145. doi: 10.1016/j.cageo.2016.07.009
- 538 Molina-Garza, R. S., Geissman, J. W., Voo, R. V. d., Lucas, S. G., & Hayden, S. N.
 539 (1991). Paleomagnetism of the Moenkopi and Chinle Formations in central
 540 New Mexico: Implications for the North America apparent polar wander path
 541 and triassic magnetostратigraphy. *Journal of Geophysical Research*, 96, 14239–
 542 14262. doi: 10.1029/91JB00644
- 543 Mullins, C. E., & Tite, M. S. (1973, Feb). Magnetic viscosity, quadrature susceptibility,
 544 and frequency dependence of susceptibility in single-domain assemblies
 545 of magnetite and maghemite. *Journal of Geophysical Research*, 78(5), 804–809.
 546 doi: 10.1029/jb078i005p00804
- 547 Néel, L. (1949). Théorie du trainage magnétique des ferromagnétiques en grains
 548 fins avec applications au terres cuites. *Annales de Géophysique*, 5(99).
- 549 Ojakangas, R. W., Morey, G. B., & Green, J. C. (2001). The Mesoproterozoic Mid-
 550 continent Rift System, Lake Superior Region, USA. *Sedimentary Geology*, 141–
 551 142, 421–442. doi: 10.1016/s0037-0738(01)00085-9
- 552 Opdyke, N. D., & DiVenere, V. J. (2004). The magnetic polarity stratigraphy of the
 553 Mauch Chunk Formation, Pennsylvania. *Proceedings of the National Academy
 554 of Sciences*, 101(37), 13423–13427. doi: 10.1073/pnas.0403786101
- 555 Özdemir, Ö., & Dunlop, D. J. (2006). Magnetic memory and coupling between spin-
 556 canted and defect magnetism in hematite. *J. Geophys. Res.*, 111(B12). doi: 10
 557 .1029/2006JB004555
- 558 Özdemir, Ö., & Dunlop, D. J. (2014). Hysteresis and coercivity of hematite.
 559 *Journal of Geophysical Research: Solid Earth*, 119(4), 2582–2594. doi:
- 560

- 566 10.1002/2013JB010739
- 567 Purucker, M. E., Elston, D. P., & Shoemaker, E. M. (1980). Early acquisition of
 568 characteristic magnetization in red beds of the Moenkopi Formation (Triassic),
 569 Gray Mountain, Arizona. *Journal of Geophysical Research*, 85(B2), 997. doi:
 570 10.1029/jb085ib02p00997
- 571 Slotznick, S. P., Swanson-Hysell, N. L., & Sperling, E. A. (2018). Oxygenated meso-
 572 proterozoic lake revealed through magnetic mineralogy. *Proceedings of the Na-*
 573 *tional Academy of Sciences*. doi: 10.1073/pnas.1813493115
- 574 Swanson-Hysell, N. L., Feinberg, J. M., Berquo, T. S., & Maloof, A. C. (2011).
 575 Self-reversed magnetization held by martite in basalt flows from the 1.1-billion-
 576 year-old Keweenawan rift, Canada. *Earth and Planetary Science Letters*,
 577 305(1-2), 171–184. doi: 10.1016/j.epsl.2011.02.053
- 578 Swanson-Hysell, N. L., Ramezani, J., Fairchild, L. M., & Rose, I. (2018). Failed
 579 rifting and fast drifting: Midcontinent Rift development, Laurentia's rapid
 580 motion and the driver of Grenvillian orogenesis. *Geological Society of America*
 581 *Bulletin*, 10.1130/B31944.1. doi: 10.1130/B31944.1
- 582 Tauxe, L., & Kent, D. (1984). Properties of a detrital remanence carried by
 583 hematite from study of modern river deposits and laboratory redeposition
 584 experiments. *Geophysical Journal of the Royal Astronomical Society*, 77,
 585 543–561. doi: 10.1111/j.1365-246X.1984.tb01909.x
- 586 Tauxe, L., & Kent, D. (2004). A simplified statistical model for the geomagnetic
 587 field and the detection of shallow bias in paleomagnetic inclinations: was
 588 the ancient magnetic field dipolar? In J. Channell, D. Kent, W. Lowrie, &
 589 J. Meert (Eds.), *Timescales of the paleomagnetic field* (Vol. 145, p. 101-116).
 590 American Geophysical Union. doi: 10.1029/145GM08
- 591 Tauxe, L., Kent, D. V., & Opdyke, N. D. (1980). Magnetic components contributing
 592 to the NRM of Middle Siwalik red beds. *Earth and Planetary Science Letters*,
 593 47, 279–284. doi: 10.1016/0012-821X(80)90044-8
- 594 Tauxe, L., Kodama, K., & Kent, D. (2008). Testing corrections for paleomagnetic
 595 inclination error in sedimentary rocks: A comparative approach. *Physics of the*
 596 *Earth and Planetary Interiors*, 169(1-4), 152–165. doi: 10.1016/j.pepi.2008.05
 597 .006
- 598 Tauxe, L., Shaar, R., Jonestrask, L., Swanson-Hysell, N., Minnett, R., Koppers,
 599 A., ... Fairchild, L. (2016). PmagPy: Software package for paleomag-
 600 netic data analysis and a bridge to the Magnetics Information Consor-
 601 tium (MagIC) Database. *Geochemistry, Geophysics, Geosystems*. doi:
 602 10.1002/2016GC006307
- 603 Van Der Voo, R., & Torsvik, T. H. (2012). The history of remagnetization of sed-
 604 imimentary rocks: deceptions, developments and discoveries. *Geological Society,*
 605 *London, Special Publications*, 371(1), 23–53. doi: 10.1144/SP371.2
- 606 Van Houten, F. B. (1968). Iron oxides in red beds. *Geological Society of America*
 607 *Bulletin*, 79(4), 399. doi: 10.1130/0016-7606(1968)79[399:ioirb]2.0.co;2
- 608 Worm, H.-U. (1998). On the superparamagnetic—stable single domain transition for
 609 magnetite, and frequency dependence of susceptibility. *Geophysical Journal In-*
 610 *ternational*, 133(1), 201–206. doi: 10.1046/j.1365-246X.1998.1331468.x
- 611 Worm, H.-U., & Jackson, M. (1999). The superparamagnetism of Yucca Mountain
 612 Tuff. *J. Geophys. Res.*, 104(B11), 25415–25425. doi: 10.1029/1999JB900285